




Aquaporin-4 Removal from the Plasma Membrane of Human Müller Cells by AQP4-IgG from Patients with Neuromyelitis Optica Induces Changes in Cell Volume Homeostasis: the First Step of Retinal Injury?

Vanina Netti¹ · Juan Fernández¹ · Luciana Melamud² · Pablo Garcia-Miranda³ · Gisela Di Giusto¹ · Paula Ford¹ · Miriam Echevarría³ · Claudia Capurro¹ 

Received: 1 May 2021 / Accepted: 11 July 2021 / Published online: 15 July 2021
© The Author(s), under exclusive licence to Springer Science+Business Media, LLC, part of Springer Nature 2021

Abstract

Aquaporin-4 (AQP4) is the target of the specific immunoglobulin G autoantibody (AQP4-IgG) produced in patients with neuromyelitis optica spectrum disorders (NMOSD). Previous studies demonstrated that AQP4-IgG binding to astrocytic AQP4 leads to cell-destructive lesions. However, the early physiopathological events in Müller cells in the retina are poorly understood. Here, we investigated the consequences of AQP4-IgG binding to AQP4 of Müller cells, previous to the inflammatory response, on two of AQP4's key functions, cell volume regulation response (RVD) and cell proliferation, a process closely associated with changes in cell volume. Experiments were performed in a human retinal Müller cell line (MIO-M1) exposed to complement-inactivated sera from healthy volunteers or AQP4-IgG positive NMOSD patients. We evaluated AQP4 expression (immunofluorescence and western blot), water permeability coefficient, RVD, intracellular calcium levels and membrane potential changes during hypotonic shock (fluorescence videomicroscopy) and cell proliferation (cell count and BrdU incorporation). Our results showed that AQP4-IgG binding to AQP4 induces its partial internalization, leading to the decrease of the plasma membrane water permeability, a reduction of swelling-induced increase of intracellular calcium levels and the impairment of RVD in Müller cells. The loss of AQP4 from the plasma membrane induced by AQP4-IgG positive sera delayed Müller cells' proliferation rate. We propose that Müller cell dysfunction after AQP4 removal from the plasma membrane by AQP4-IgG binding could be a non-inflammatory mechanism of retinal injury *in vivo*, altering cell volume homeostasis and cell proliferation and consequently, contributing to the physiopathology of NMOSD.

Keywords Aquaporin 4 · AQP4-IgG · Human Müller cells · Cell volume regulation · Cell proliferation

Introduction

Neuromyelitis optica spectrum disorders (NMOSD) is a devastating, inflammatory, and demyelinating disease of the central nervous system (CNS) that preferentially affects the optic nerves and spinal cord [1]. The majority of patients are seropositive for a highly specific serum immunoglobulin G that targets Aquaporin-4 (AQP4), called AQP4-IgG [2, 3]. AQP4 is the major plasma membrane water channel in the CNS and it is highly expressed in the polarized plasma membrane of astrocytic endfeet facing the blood–brain barrier as two major isoforms (M1 and M23), which are organized in structures known as orthogonal arrays of particles (OAPs) [4]. Clinical and pathological studies have proposed that AQP4-IgG binding to astrocytic AQP4 produces complement-dependent cytotoxicity, which leads to astrocyte-destructive lesions in the spinal cord and optic nerves [5, 6].

✉ Claudia Capurro
capurroclaudia@yahoo.com.ar

¹ Departamento de Ciencias Fisiológicas, Laboratorio de Biomembranas, Facultad de Medicina, Instituto de Fisiología y Biofísica “Bernardo Houssay” (IFIBIO-HOUSSAY), Consejo Nacional de Investigaciones Científicas Y Técnicas (CONICET), Universidad de Buenos Aires, Buenos Aires, Argentina

² Servicio de Neurología, Centro Universitario de Neurología Dr. J.M. Ramos Mejía, Facultad de Medicina, Universidad de Buenos Aires, Buenos Aires, Argentina

³ Instituto de Biomedicina de Sevilla (IBiS), Hospital Universitario Virgen del Rocío/CSIC, Universidad de Sevilla, Seville, Spain

However, other evidence indicates that AQP4-IgG can also induce complement-independent pathogenesis, suggesting that different mechanisms of AQP4-IgG may act concurrently [7, 8].

In addition to astrocytes, AQP4 is also highly expressed in Müller cells in the inner retina and in glial membranes contacting retinal ganglion cells as well as in nerve fibers [9]. Using optical coherence tomography (OCT), several studies demonstrated that damage to optic nerves in NMOSD is also associated with retinal injury [10–13]. Other reports demonstrate that NMOSD patients AQP4-IgG-seropositive without a medical history of optic neuritis have microstructural changes in the fovea region, a retinal site rich in Müller cells, supporting the proposal of Müller cells as a target of AQP4-IgG [14] and that subclinical anterior visual pathway involvement may occur in AQP4-IgG + NMOSD [15]. However, until a few years ago, there was no direct evidence about an association between AQP4-IgG and the presence of retinal lesions in patients with NMOSD [16]. Intravitreal injection to adult rats retina of a monoclonal AQP4-specific recombinant antibody derived from an NMOSD patient (rAb-53) showed that, in fact, the antibody efficiently bound to AQP4 on retinal Müller cells and produced complement-independent retinal injury [17]. Nevertheless, as AQP4-IgG is a polyclonal autoantibody that binds multiple epitopes with variable avidity for them [1], the effects of NMOSD patients' sera on Müller cells warrant further study.

One of the major functional roles of Müller cells is to maintain extracellular fluid and ionic homeostasis within the retina since neural activity alters osmotic gradients leading to cell swelling, which is followed by a regulatory volume decrease (RVD) response, in which AQP4-mediated water transport would play an active role [18]. We have previously reported that RVD in Müller cells is a complex response that involves Transient Receptor Potential Vanilloid 4 (TRPV4) calcium channel-dependent changes in membrane potential (V_m) as well as the activation of K^+ and Cl^- channels and the release of amino acids such as Taurine and Glutamate via the Volume Regulated Anion Channel (VRAC) [19–21]. Even more, previous reports in astrocytes showed a physical and functional interaction between TRPV4 and AQP4, necessary for RVD activation [22] and it was proposed that AQP4-TRPV4 interactions constitute a molecular system that finetune astroglial volume regulation by integrating osmosensing, calcium signaling, and water transport, and when over-activated, they can trigger pathological swelling [23]. However, the consequences of AQP4-IgG binding to AQP4 on RVD machinery were not investigated in Müller cells, in particular the putative involvement of TRPV4 in NMOSD physiopathology.

Another important role of Müller cells is to maintain retinal integrity. These cells respond to injury by a mechanism known as reactive gliosis, which involves the activation of

the cell cycle and subsequent dedifferentiation to other cell types, having a role of stem cells in the adult retina [24–26]. Interestingly, stem cell transplantation has been considered to be a potential treatment method for neurological disorders including NMOSD [27]. In addition, it was proved that AQP4 affects cell proliferation in different cell types [28, 29] and several AQPs have a role in cell proliferation by acting through various different mechanisms, specifically, by allowing fast cell volume regulation during cell division, by affecting the progression of the cell cycle, and by crosstalking with other cell membrane proteins or transcription factors that, in turn, modulate the progression of the cell cycle [30, 31]. Therefore, the aim of this study was to investigate whether the binding of AQP4-IgG to AQP4 in Müller cells will threaten cell volume regulatory capacity and consequently cell proliferation. We used a human retinal Müller cell line (MIO-M1), a model that expresses endogenous AQP4 and maintains important functional characteristics of Müller cells [32] exposed to decompensated AQP4-IgG positive sera from different NMOSD patients, to prevent complement-dependent cytotoxicity. Our results showed that endocytosis of AQP4, after binding of AQP4-IgG, affects Müller cells RVD capacity altering cell volume control and delaying proliferation rate, probably contributing to the physiopathology of NMOSD. Understanding these mechanisms will pave the way for therapeutic interventions in this disease.

Material and Methods

Cell Cultures

The MIO-M1 cell line (kindly provided by Dr. Astrid Limb, University College London, London, UK) is a spontaneously immortalized retinal Müller glial cell line, originated from human retina that retained many characteristics of Müller cells [32]. Cells were grown as monolayers in the presence of Dulbecco's Modified Eagle Medium (DMEM)/glutamax supplemented with 10% fetal calf serum (FCS), with 5 μ g/ml streptomycin and 5 U/ml penicillin at 37 °C in a humidified atmosphere containing 5% CO_2 . Cells were routinely subcultured every week. For immunofluorescence and functional studies, MIO-M1 cells were seeded on glass coverslips (12 mm diameter) at 5–10 $\times 10^3$ cells/ml densities, for 48 h and then subjected to the different experimental conditions.

Patients and Serum Samples

Serum samples were collected from patients that fulfilled the original diagnostic criteria for NMO and were AQP4-IgG positive, as previously described [33], from the Neuro-immunologic Clinic Service of the Ramos Mejia Hospital,

Argentina, and from the Neurology Department at the Virgen of Rocío University Hospital (HUVR), Spain. As control, we included serum from healthy AQP4-IgG negative volunteers. All subjects signed the informed consent form, and the study was approved by the Institutional Review Boards and conducted in compliance with the Declaration of Helsinki. Demographic and clinical characteristics of patients included in our study were previously reported [34, 35]. Sera were stored at $-80\text{ }^{\circ}\text{C}$ and complement was inactivated holding 30 min at $56\text{ }^{\circ}\text{C}$.

Cells Pretreatment with Control or Patient Sera

MIO-M1 human Müller cells were exposed to control or patients heat-inactivated sera (dilution 1/50 in culture media) for 1 h at $4\text{ }^{\circ}\text{C}$ or 12 h at $37\text{ }^{\circ}\text{C}$. These conditions were selected to avoid or to facilitate AQP4 downregulation, respectively, as previously described in HEK-293 cells and astrocytes primary culture [34, 36]. After these treatments, cells were washed with PBS and then immunofluorescence or functional studies were performed. As a control for AQP4 function in Müller cells, in some experiments, cells were preincubated with 100 nM of the specific AQP4 inhibitor *N*-1,3,4-Thiadiazol-2-yl-3-pyridinecarboxamide (TGN-020, Sigma-Aldrich) [37] in the isoosmotic extracellular solution and the same concentration was used throughout the experiments.

Measurement of Cell Volume Changes, Water Permeability, RVD Response, and Intracellular Calcium Levels

MIO-M1 cells were seeded on glass coverslips (12 mm diameter) at $5\text{--}10 \times 10^3$ cells/mL densities for 48 h. Before the experiments, the coverslips were incubated in the experimental buffer at $20\text{ }^{\circ}\text{C}$ for at least 15 min. As previously reported, we simultaneously recorded changes in cell volume and intracellular calcium levels ($[\text{Ca}^{2+}]_i$) in single cells by incubating cells for 60 min at $37\text{ }^{\circ}\text{C}$ with $14\text{ }\mu\text{M}$ of the calcium-sensitive dye FURA-2 AM (Invitrogen, Thermo Fisher Scientific) [20]. Fluorescence was recorded at the calcium-sensitive (380 nm) and -insensitive (358 nm, isosbestic) wavelengths. Changes in cell volume were read from the fluorescence intensity recorded at 358 nm and changes in $[\text{Ca}^{2+}]_i$ were obtained from the ratio of 358/380 (R_t/R_0 Fura-2) with a Nikon TE-200 epifluorescence inverted microscope (Nikon Planfluor $\times 40$ oil immersion objective lens), coupled to a device camera (Hamamatsu C4742-95), and connected to a computer with the Metafluor software acquisition program (Universal Imaging Corporation, PA) [19]. Cells were exposed to hypotonic shock and relative fluorescence (F_t/F_0) was obtained. F_0 represents the pinhole signal when placed in equilibrium with an iso-osmotic medium with an

osmolality OsM_0 (300 mOsM) and F_t is the fluorescence from the same region at time t , when placed in equilibrium with a solution with an osmolality of OsM_t . Changes in cell volume can be calculated as follows:

$$\frac{V}{V_0} = \frac{\left(\frac{F_0}{F_t}\right) - f_b}{1 - f_b}$$

where V is cell volume at time t ; V_0 is cell volume at $t=0$; and f_b is the relative background. This parameter corresponds to the y intercept of a plot of F_0/F_t versus $\text{OsM}_0/\text{OsM}_t$, which represents relative fluorescence in the absence of osmolality changes.

RVD after cell exposure to a hypo-osmotic medium was calculated by the following equation:

$$\%RVD_{15} = \left[\frac{\left(\frac{V}{V_0}\right)_{\max} - \left(\frac{V}{V_0}\right)_{15}}{\left(\frac{V}{V_0}\right)_{\max} - 15} \right] \times 100$$

where $(V/V_0)_{\max}$ is the maximal value of V/V_0 attained during hypo-osmotic swelling (peak), and $(V/V_0)_{15}$ represents the value of V/V_0 observed at time 15 min after the osmotic shock. $\%RVD_{15}$ thus denotes the magnitude of volume regulation 15 min after the osmotic shock, with 100% RVD indicating complete volume regulation and 0% RVD indicating no volume regulation.

Osmotic water permeability of MIO-M1 cells was estimated from the time course of V/V_0 during the first 2 min. Curves for each experiment were fitted with a single exponential function with the software GraphPad Prism 6.0 and the osmotic water permeability coefficient (P_f) was calculated from the exponential time constant (τ) by the equation:

$$P_f = \frac{V_0}{\tau \cdot A \cdot \text{OsM} \cdot V_w}$$

where V_0 is the initial cell water volume; A is the cell surface area; OsM is the osmotic gradient; and V_w is the partial molar volume of water ($18\text{ cm}^3\text{ mol}^{-1}$). Volume-area relation (V_0/A) of MIO-M1 cells was calculated from confocal images using the Imaris 7.1.0 software (Bitplane) with a mean value, in $\text{cm} \cdot 10^{-5}$, of 20.85 ± 0.70 ($n=27$).

Measurement of Membrane Voltage Changes

Transmembrane potential was measured using DIBAC₄(3), a slow response anionic dye whose emission is independent of cell volume changes, as previously shown in Müller cells [19, 20]. Cells were loaded with $2.5\text{ }\mu\text{M}$ DIBAC₄(3) for 15 min at $20\text{ }^{\circ}\text{C}$ and placed on the stage of the same microscope described in the previous section. Excitation wavelength was 490 nm and emitted light (above 520 nm)

was recorded at 10-s intervals. Fluorescence intensity was monitored until it reached a stable value before starting the experiments. Fluorescence intensity changes after interventions were relativized to stationary values (F_i/F_0) and data were corrected for background noise and drift.

Immunofluorescence Assays and Quantification of AQP4

For AQP4 detection after control or AQP4-IgG + sera treatment, MIO-M1 cells were fixed in 4% paraformaldehyde for 1 h and then permeabilized with 1% glycine and 0.1% Triton X-100 at room temperature. Samples were blocked with 5% Fetal Bovine Serum for 2 h and sequentially incubated with a rabbit polyclonal anti-AQP4 antibody (1/1000) directed against an epitope located at the intracellular C-terminal domain of rat AQP4 to amino acid residues 249–323 (#AQP-004, Alomone Labs) overnight at 4 °C and a secondary antibody (rabbit anti-Cy3 conjugate, dilution 1:100, Jackson Immuno 111–165-003) for 2 h at room temperature. Then, nuclei were stained with Hoechst (5 µg/ml) for 1 min. Coverslips were mounted with Vectashield mounting medium. Images were captured using epifluorescence on an Olympus FluoView FV1000 confocal microscope and digitalized. The intensity of AQP4-Cy3 fluorescence was quantified by densitometry using the ImageJ software and then analyzed using the formula:

$$\sum_n IF(n)$$

where n stands for the number of optical sections required scanning the entire cell, and $IF(n)$ stands for integrated fluorescence intensity within a given optical section.

To quantify AQP4 at the plasma membrane in MIO-M1 cells, immunofluorescence studies were performed using the same technique but before fixation, cells were incubated for 30 min at 4 °C with Alexa Fluor® 488-conjugated wheat germ agglutinin (WGA-488; Thermo Fisher Scientific Cat# W11261) that selectively binds to *N*-acetylglucosamine and *N*-acetylneuraminic acid residues and can be used to label glycoproteins for imaging the plasma membrane. In other experiments, to evaluate the presence of intracellular AQP4 in early endosomes, double immunostaining was performed by using anti-early endosome antigen 1 (EEA1) mouse monoclonal antibodies (1/300, BD Biosciences) and anti-AQP4 antibodies, as described above. Confocal images were analyzed by using ImageJ colocalization tools and estimated using the M2 superposition coefficient of Manders (SCM), which measures the fraction of WGA/EEA1 that overlaps AQP4 signal, and is described by the following equation:

$$SCM = \frac{\sum_i (R_i \times G_i)}{\sqrt{\sum_i R_i^2 \times G_i^2}}$$

where R and G are the average intensities for the red and green channel signal, respectively. A value of 1 indicates 100% of superposition between signals of colocalized pixels, while a value of 0 indicates absence of pixel colocalization.

For TRPV4 immunostaining, the same protocol was applied and an anti-TRPV4 antibody was used (1/1500; Alomone Labs, #ACC-034). Since plasma membrane TRPV4 expression was low, to identify its presence, we created a mask of plasma membrane as previously described [20]. Briefly, WGA images were binarized so that the signal from WGA was ascribed the value of “1” and the rest of the image was ascribed the value of “0.” The Boolean logical operation “AND” was then performed on the corresponding images, representing signals from TRPV4-Cy3 and from WGA (binary mask). This resulted in generation of a new image (shown in yellow in the figures) corresponding to the TRPV4-Cy3 fluorescent signal corresponding to the plasma membrane.

Western Blotting

Confluent MIO-M1 cells seeded in T25 bottles were washed three times in cold PBS and were incubated for 30 min at 4 °C in RIPA Lysis buffer containing 150 mM NaCl, 50 mM Tris/HCl pH 7.5, 0.5 g % sodium deoxycholate, 0.1 g % SDS, 2.5 mM EDTA, 1% Triton 100, 1 mM PMSF, 5 µg/ml aprotinin, 10 µg/ml antipain, 10 µg/ml leupeptin, and 10 µg/ml pepstatin. Cells were then collected with a rubber scraper, homogenized, and sonicated. Whole cell lysates were obtained by centrifugation at 10,000 g at 4 °C for 10 min. For plasma membrane enrichment, confluent MIO-M1 cells seeded in T75 bottles were the cells were subjected to the same treatment plus an additional centrifugation was performed at 17,000 g at 4 °C for 45 min as previously described [38]. Samples were then subjected to electrophoresis in 12% SDS–polyacrylamide gel (Bio-Rad), transferred to a nitrocellulose membrane (Bio-Rad), and blocked 1 h with 5% non-fat dried skimmed milk. Membranes were then incubated with the rabbit polyclonal anti-AQP4 antibody (1/1000, #AQP-004, Alomone Labs) overnight at 4 °C. The blots were then washed and incubated 1 h at room temperature with an anti-mouse IgG conjugated to horseradish peroxidase (dilution 1:7500, Sigma-Aldrich). Membranes were visualized using the chemiluminescence method (SuperSignal Substrate, Pierce) and captured on a Gbox (Syngene).

Proliferation Assays

For cell count, MIO-M1 cells were seeded in a 24-well plate at a concentration of 24,000 cells/ml. Control or AQP4-IgG + sera were added 24 h after seeding and these experimental conditions were maintained during the whole experiment. At each experimental time (0 to 72 h), the cells were harvested by trypsinization, resuspended in Trypan blue to exclude non-viable cells and estimate cell viability, and counted on a hemocytometer (Neubauer chamber). Cell doubling time was obtained after adjusting the results to an exponential function using the GraphPad Prism 6 software.

For cell proliferation analysis, MIO-M1 cells were pulsed with 20 mM of the thymidine analog 5-Bromodeoxyuridine (BrdU; Sigma-Aldrich) for 1 h. Cells were fixed in 3% paraformaldehyde for 30 min and then neutralized with NH_4Cl 50 mM/PBS for 15 min. BrdU content was analyzed after DNA denaturation with 2 N HCl and 0.1% Triton X-100 at room temperature, followed by neutralization with 0.1 M $\text{Na}_2\text{B}_4\text{O}_7$ pH 8.5. The cells were labeled using specific anti-BrdU monoclonal antibodies (Sigma-Aldrich) and Cy2-conjugated secondary antibodies (Jackson Immuno, Pennsylvania, PA). For PI counter-staining, cells were washed twice with PBS and incubated in the presence of PI (50 mg/ml) in PBS for 10 min in the dark. The percentage of proliferating cells was calculated from the quantification of the total cells stained with IP (red channel) and the positive BrdU (green channel) using an Olympus IMT-2 inverted microscope and the ImageJ software (National Institute of Health).

Solutions and Chemicals

For functional experiments, cells were first set, for at least 10 min, in an external iso-osmotic solution containing (mM): 126 NaCl; 5.5 KCl; 2.5 CaCl_2 ; 1.25 MgCl_2 ; 20 Hepes; and 10 glucose (osmolarity: 299 ± 2 mOsM). Hypo-osmotic solutions were prepared from iso-osmotic solution by the removal of NaCl to create an osmotic gradient of 100 mOsM. All solutions were titrated to pH 7.40 using NaOH (Sigma-Aldrich), and osmolalities were routinely measured by a pressure vapor osmometer (Wescor). Cells were pre-incubated in an iso-osmotic extracellular solution containing drugs or vehicle (DMSO). 1 mM FURA-2 AM and 0.6 mM DIBAC₄(3) stock solutions were prepared in DMSO and stored at -20 °C until used.

Statistics

Data were evaluated with either Student's *t* test or one-way analysis of variance (ANOVA) followed by Bonferroni's post hoc test for multiple comparisons. Bonferroni correction for multiple comparisons (significance cut-off at α/n , being α the level of significance, usually 0.05, and *n*

the number of hypotheses to be tested) was applied when appropriate. Values are reported as mean \pm SEM, and *n* is either the number of cells evaluated in each condition or the number of experiments. All statistical procedures were performed using GraphPad Prism 6.0 statistical software package.

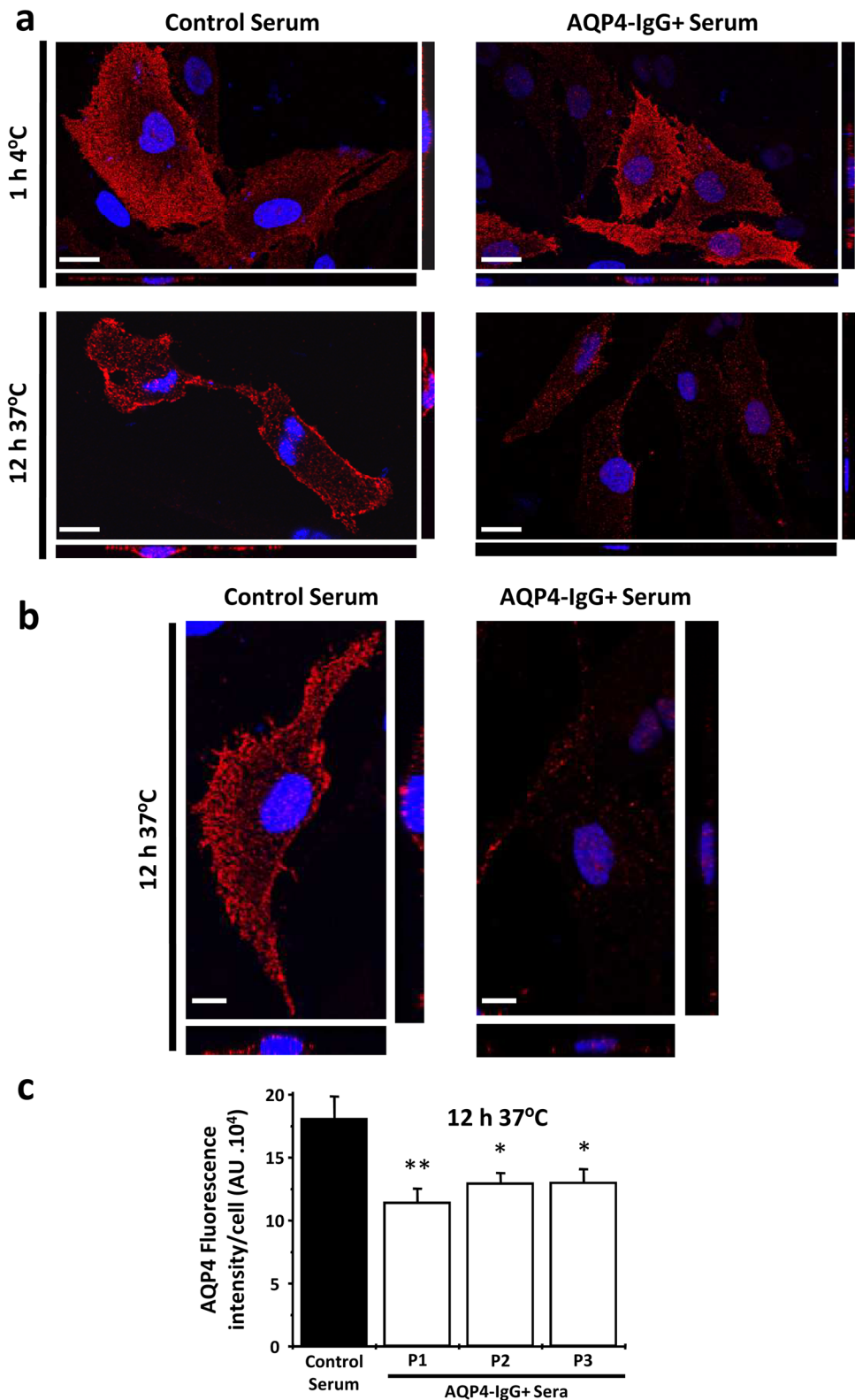
Results

Long-Term Exposure to AQP4-IgG Reduces AQP4 Plasma Membrane Expression in Müller Cells

We and others have previously reported that long-term exposition to AQP4-IgG positive (AQP4-IgG+) serum induced AQP4 internalization in rat astrocytes [34, 39]. In the present study, we analyzed, for the first time, the effects of the binding of AQP4-IgG + serum from NMO/MS patients to AQP4 expressed in human Müller cells. For this, MIO-M1 cells were exposed to control or AQP4-IgG + sera for 1 h at 4 °C or 12 h at 37 °C, to avoid or to facilitate AQP4 down-regulation, respectively [34, 39]. Figure 1a resumes representative confocal immunofluorescence experiments, using a polyclonal anti-AQP4 antibody, showing that after exposure of cells for 1 h at 4 °C to control or AQP4-IgG + sera, AQP4 remained largely expressed in the cell membrane. In contrast, exposure to AQP4-IgG + serum for 12 h at 37 °C reduced the AQP4 signal. Figure 1b shows magnification of confocal images, where it can be noted that a laminar and continuous AQP4 signal was observed after control sera exposure, which became in a very slight and point-shaped staining pattern after AQP4-IgG treatment. Figure 1c illustrates the quantification of total AQP4 expression in MIO-M1 cells (plasma and intracellular membranes) after exposition at 37 °C for 12 h to AQP4-IgG + sera from three different NMO/MS patients. It can be observed that after the incubation, a significant reduction of AQP4 expression occurs in comparison to cells exposed to control serum.

To confirm whether AQP4 was in fact removed from the plasma membrane when MIO-M1 cells were exposed to AQP4-IgG + serum for 12 h at 37 °C, we studied AQP4 colocalization with the plasma membrane marker WGA by confocal immunofluorescence. As shown in Fig. 2a, when cells were incubated with control serum, AQP4 was largely expressed at the plasma membrane. However, when exposed to AQP4-IgG + serum, AQP4 plasma membrane expression was largely reduced, as evidenced by the Mander's overlap coefficient (control serum vs AQP4-IgG + serum: 0.677 ± 0.043 vs. 0.349 ± 0.064 , $n = 3-4$ experiments, $p < 0.005$). In agreement with this, Western blot analysis revealed that the major band for AQP4 expressed at the plasma membrane of Müller cells (~ 40 kDa) was significantly reduced after treatment with

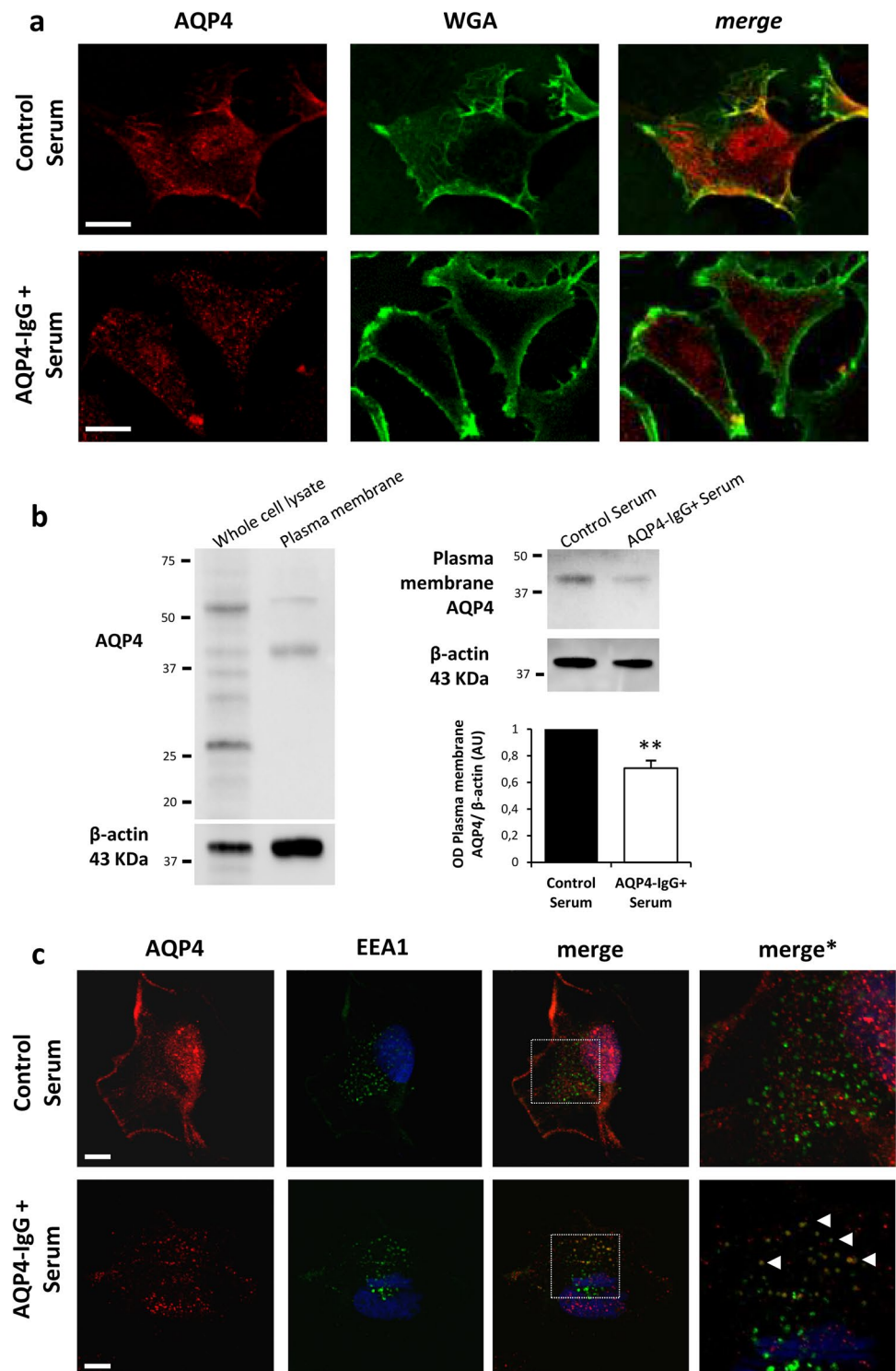
Fig. 1 AQP4 expression in MIO-M1 cells after exposure to control or AQP4-IgG positive sera. **a** Cells were treated for 1 h at 4 °C or 12 h at 37 °C with control or AQP4-IgG + sera and then immunofluorescence experiments were performed using a polyclonal anti-AQP4 antibody (red). Top panel: confocal images illustrating similar staining pattern of plasma membrane AQP4 after exposure to control or AQP4-IgG + sera for 1 h at 4 °C. Lower panel: confocal images illustrating changes in the staining pattern after exposure for 12 h at 37 °C to AQP4-IgG + serum, compared to control serum. Images are representative of three independent experiments (scale bars: 20 μm). **b** Detailed magnification of cells exposed to control or AQP4-IgG + sera for 12 h at 37 °C (scale bars: 10 μm). **c** Total fluorescence quantification of positively-stained cells after incubation for 12 h at 37 °C with control or 3 different AQP4-IgG + sera exposure. Immunofluorescence values per cell (AU: arbitrary units) are expressed as mean ± SEM for 23–52 cells from 3 experiments for each condition ***p* < 0.01 and **p* < 0.05 control vs. AQP4-IgG + sera



AQP4-IgG + serum at 37 °C for 12 h, in comparison to cells exposed to control serum (Fig. 2b). To further evaluate the internalization of AQP4 after AQP4-IgG binding in Müller cells, we performed immunolocalization

experiments of AQP4 and the early endosome antigen 1 (EEA1), which localizes exclusively to early endosomes and was shown to colocalize with AQP4 in astrocytes [39]. Figure 2c shows an increased localization of AQP4

Fig. 2 AQP4 expression and localization in plasma membrane of MIO-M1 cells after exposure to control or AQP4-IgG positive sera. **a** Immunofluorescence confocal images of MIO-M1 cells stained with a polyclonal anti-AQP4 antibody (red), WGA plasma membrane staining (green), and merge of both images (yellow) after treatment for 12 h at 37 °C with control (upper panel) or AQP4-IgG + sera (lower panel). Images are representative of three independent experiments (scale bars: 20 μ m). **b** Western blot showing the expression of several AQP4 isoforms in whole cell lysates and in enriched plasma membrane fractions (left) and AQP4 plasma membrane expression after treatment for 12 h at 37 °C with control or AQP4-IgG + sera (right). Values are expressed as mean \pm SEM, $**p < 0.01$ control vs. AQP4-IgG + sera. **c** Immunofluorescence confocal images of MIO-M1 cells stained with a polyclonal anti-AQP4 antibody (red), EEA1 (green), and merge of both images (yellow) after treatment for 12 h at 37 °C with control (upper panel) or AQP4-IgG + sera (lower panel). Images are representative of three independent experiments (scale bars: 10 μ m). Merge* show enlarged boxed areas from merged image



in early endosomes after exposure to AQP4-IgG + serum (merge*, indicated by arrows), which was also evidenced by Mander's overlap coefficient (control serum vs AQP4-IgG + serum: 0.315 ± 0.062 vs. 0.874 ± 0.085 , $n = 3$ experiments, $p < 0.01$).

Altogether, these results support the partial internalization of AQP4 expressed in the plasma membrane of Müller cells into the endosomal compartment following long-term exposure to AQP4-IgG + sera.

AQP4 Internalization by Long-Term Exposure to AQP4-IgG Reduces Müller Cells Water Permeability and RVD Capacity

We next investigated the functional consequences of Müller cells' treatment with control or NMOSD patients' sera for 1 h at 4 °C or 12 h at 37 °C. For this purpose, we measured the time course of MIO-M1 cell swelling (V/V_0) in response to an osmotic gradient (ΔOsM : 100 mOsM) by fluorescence videomicroscopy using FURA-2 AM. Figure 3a shows a similar swelling kinetics of V/V_0 in cells exposed to control or AQP4-IgG + sera for 1 h at 4 °C, without differences

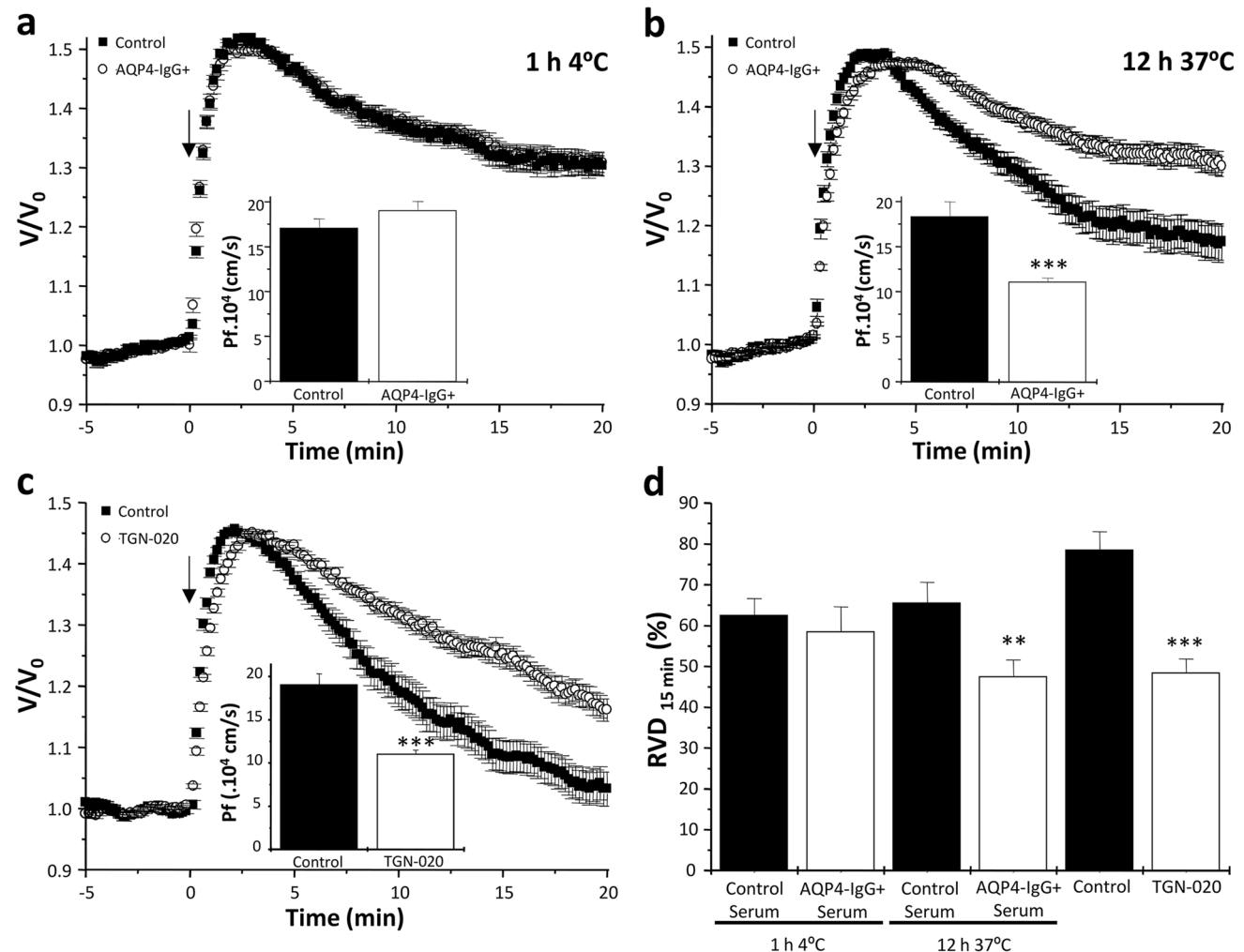


Fig. 3 Osmotic water permeability and RVD response of MIO-M1 cells after exposure to control or AQP4-IgG positive sera. **a–c** Time course of the relative cell volume (V/V_0) after exposure of cells to a hypoosmotic gradient (ΔOsM =100 mOsM, indicated by arrows) in MIO-M1 cells treated with control or AQP4-IgG sera for 1 h at 4 °C (**a**) and for 12 h at 37 °C (**b**) or in the presence of AQP4 inhibitor TGN-020 100 nM or its vehicle (control) (**c**). Inserts show the osmotic water permeability (Pf) estimated from the time course of V/V_0 during the first 2 min after the hypotonic shock in all experi-

mental conditions. Values are expressed as mean \pm SEM from 48–58 cells of 4–5 experiments, *** p < 0.001, control serum vs. AQP4-IgG + serum; *** p < 0.001 control vs. TGN-020. **d** MIO-M1 cells RVD response 15 min after the maximal osmotic swelling (% RVD15 min) in all experimental conditions. Values are expressed as mean \pm SEM from 48–58 cells of 4–5 experiments; ** p < 0.01, control serum vs. AQP4-IgG + serum; *** p < 0.001 control vs. TGN-020

in osmotic water permeabilities (Pf, insert), demonstrating that the binding of AQP4-IgG to AQP4 does not directly inhibit water channel function. The lack of ability of AQP4-IgG + serum to inhibit water permeability was further demonstrated comparing these results with those obtained by using the novel specific AQP4 inhibitor TGN-020. Our results showed that when AQP4 expressed in Müller cells is blocked with 100 nM TGN-020, Pf was significantly reduced (Fig. 3c). In contrast, Fig. 3b shows that exposure of Müller cells to AQP4-IgG + serum for 12 h at 37 °C significantly delayed cell swelling kinetics, compared to control serum, which can be explained by a reduction of the osmotic water

permeability. In addition, Fig. 3d shows the percentage of RVD response 15 min after the hypotonic shock ($RVD_{15\text{ min}}$) in the three experimental conditions previously described. The $\% RVD_{15\text{ min}}$ was comparable between cells exposed to control or AQP4-IgG + sera for 1 h at 4 °C. However, the capacity of Müller cells to regulate its volume after an osmotic swelling was significantly decreased after exposure for 12 h at 37 °C to AQP4-IgG compared to control serum, as well as by TGN-020 treatment compared to vehicle.

We have previously reported that the magnitude of changes in intracellular calcium levels after cell swelling determine the efficiency of RVD in Müller cells [20]. Then, we next evaluated the time course of relative changes in calcium levels (R_t/R_0 Fura-2 AM) during a hypoosmotic shock in cells exposed for 12 h at 37 °C to control or AQP4-IgG + sera. It can be observed that, in cells treated with AQP4-IgG + sera, the cell swelling-induced increase in calcium levels was reduced and delayed compared to control sera (Fig. 4a, c, d). Similar results were obtained by blocking

AQP4 with TGN-020, which also provoked a decrease of the swelling-induced calcium maximal levels and increased time to peak (Fig. 4b, c, d). However, no differences were observed in hypotonicity-induced changes in calcium levels of MIO-M1 cells exposed to control or AQP4-IgG + sera for 1 h at 4 °C (data not shown).

Altogether, these results strongly suggest that AQP4-IgG does not impair AQP4 function as a water channel, but causes its internalization with the consequent reduction of water permeability and the efficiency of the RVD response in Müller cells.

TRPV4 Activity Is not Affected by Long-Term Exposure to AQP4-IgG in Müller Cells

We have previously reported that the calcium channel TRPV4 modulates the changes in V_m occurring during RVD [20]. These evidence, together with the demonstration that TRPV4 and AQP4 channels synergistically regulate

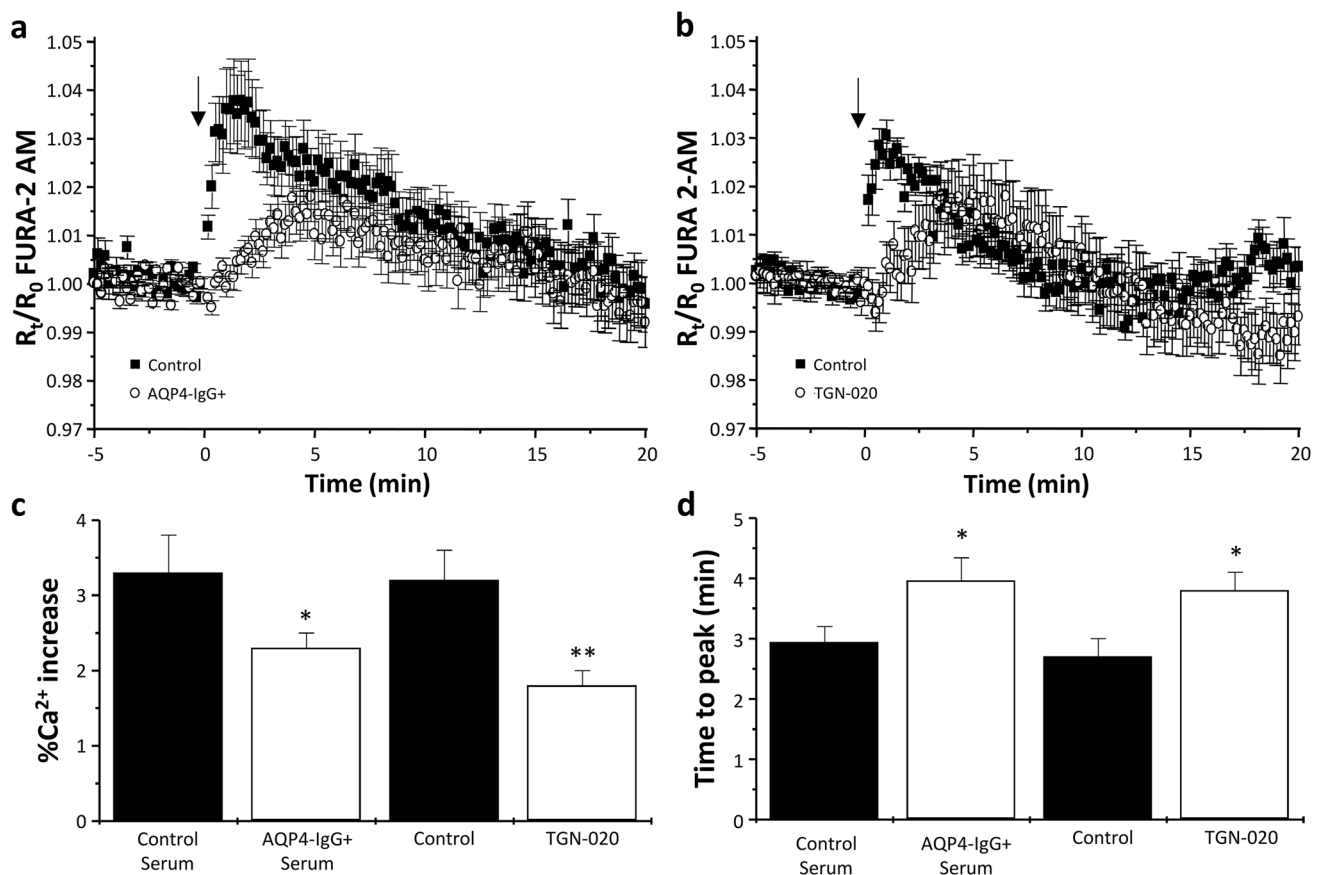


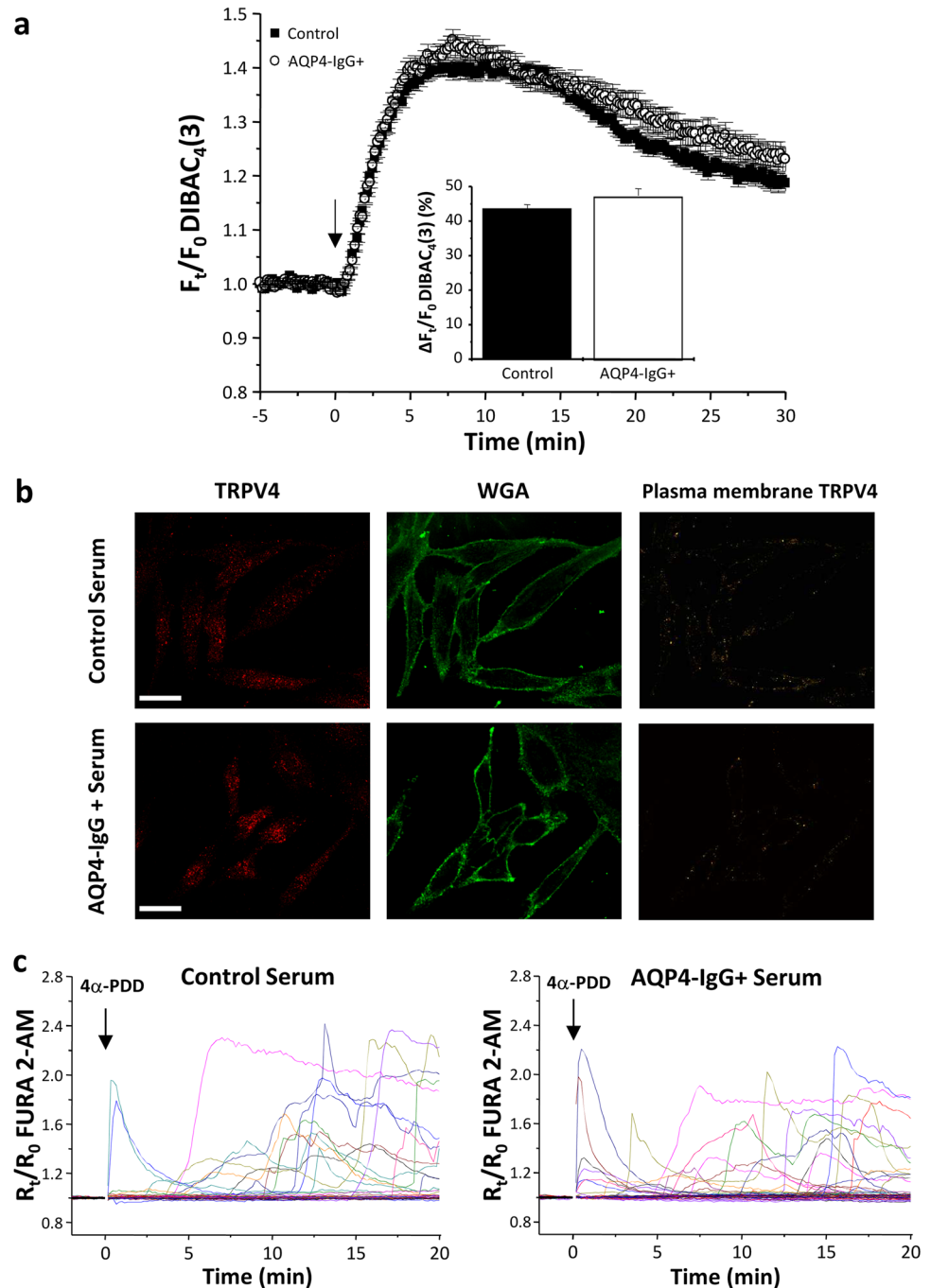
Fig. 4 Changes in intracellular calcium levels during hypotonic shock and RVD in Müller cells after exposure to control or AQP4-IgG positive sera. Cells were treated for 12 h at 37 °C with control or AQP4-IgG + sera (a) or AQP4 inhibitor TGN-020 100 nM or its vehicle (control) (b). Then, they were loaded with FURA-2 AM to measure intracellular calcium levels and exposed to a hypoosmotic gradient

($\Delta OsM = 100$ mOsM, indicated by arrows). **a–b** Kinetics of intracellular Ca^{2+} levels measured as the ratio 358/380 (R_t/R_0 FURA-2 AM). **c** Maximal change in Ca^{2+} increase (%). **d** Time to peak (min). Values are expressed as mean \pm SEM for 45–53 cells from 4–5 independent experiments; * $p < 0.05$ control serum vs. AQP4-IgG + serum/TGN-020; ** $p < 0.01$ control vs. TGN-020

cell volume in retinal Müller glia [23], led us to investigate if the endocytosis of AQP4 by AQP4-IgG may also affect TRPV4 activity in Müller cells. For this, MIO-M1 cells were exposed to control or AQP4-IgG + sera for 12 h at 37 °C, and then, Vm and TRPV4 expression and activity were measured. Regarding changes in Vm occurring during cell swelling and RVD by videomicroscopy using DIBAC₄(3) (F_t/F_0), we observed that Vm was not affected by AQP4-IgG + sera compared with control sera (Fig. 5a). Figure 5b confirms that the expression of TRPV4 was unaffected after exposure

to AQP4-IgG + sera for 12 h at 37 °C. In fact, using an anti-TRPV4 antibody (red) and the plasma membrane marker WGA (green), we observed no changes in colocalized plasma membrane signals (yellow). In addition, we tested TRPV4 function by its activation with the specific agonist 4 α -PDD (10 μ M) in isotonic conditions. Figure 5c shows the kinetics of intracellular calcium levels, where the percentage of responding cells (~50% in each condition) exhibited a similar time to peak (control: 12.9 \pm 1.3 vs. AQP4-IgG: 10.0 \pm 1.5 min, n = 25–30 cells of 4–5 experiments,

Fig. 5 Changes in membrane potential during hypotonic shock and TRPV4 expression and function of MIO-M1 cells after exposure to control or AQP4-IgG positive sera. **a** Kinetics of DIBAC₄(3) relative fluorescence (F_t/F_0). Cells were treated for 12 h at 37 °C with control or AQP4-IgG + sera, loaded with DIBAC₄(3) to measure membrane potential changes and then exposed to a hypoosmotic gradient (Δ OsM = 100 mOsM, indicated by arrows). Inserts show the maximal change in F_t/F_0 DIBAC₄(3). Values are expressed as mean \pm SEM for 42–57 cells from 4–5 independent experiments. **b** Immunofluorescence confocal images of MIO-M1 cells stained with a polyclonal anti-TRPV4 antibody (red), WGA plasma membrane staining (green), and plasma membrane TRPV4 (yellow) after treatment for 12 h at 37 °C with control (upper panel) or AQP4-IgG + sera (lower panel). Images are representative of three independent experiments (scale bars: 30 μ m). **c** Kinetics of intracellular Ca²⁺ levels measured as the ratio 358/380 (R_t/R_0 FURA-2 AM) of MIO-M1 cells measured before and after specific TRPV4 activation with 10 μ M 4 α -PDD (indicated by arrows) in isotonic conditions in cells pretreated with control (left) or AQP4-IgG + sera (right) for 12 h at 37 °C



ns) and percentage of maximal increase in calcium levels (control: 72.2 ± 8.6 vs. AQP4-IgG: $60.4 \pm 6.5\%$, $n = 25$ –30 cells of 4–5 experiments, ns). These results strongly suggest that TRPV4 activity/expression is not impaired by AQP4-IgG + sera in Müller cells.

Cell Proliferation Is Affected by Long-Term Exposure to AQP4-IgG

We next evaluated if the observed RVD impairment due to AQP4-IgG binding to AQP4 may affect cell proliferation, a process closely associated with cell volume changes. For this, we first evaluated the kinetics of cell growth in MIO-M1 cells after incubation up to 72 h with control or AQP4-IgG + sera from three different patients. It can be noticed that the cells exposed to AQP4-IgG decreased their rate of growth in comparison to those exposed to the control sera, which is reflected by a significant increase in the period of time required for cells to double in number (Fig. 6a and b). Similar results were obtained when MIO-M1 cells were incubated with the inhibitor TGN-020, demonstrating that AQP4 is involved in the proliferation of Müller cells, as previously shown in other cell types (Fig. 6b). Importantly, these changes in cell growth are not due to cell death since cell viability, assessed by Trypan Blue exclusion method, was not affected by the presence of AQP4-IgG compared to the control sera or in the presence of TGN-020 (control vs AQP4-IgG + sera: 95 ± 2 vs. 93 ± 3 , $n = 4$ –5 experiments, ns and control vs. TGN-020: 92 ± 2 vs. 94 ± 1 , $n = 4$ –5 experiments, ns).

We further evaluated MIO-M1 cell proliferation in the presence of control or AQP4-IgG + sera by measuring the incorporation of the thymidine analog 5-Bromodeoxyuridin (BrdU) as a marker of DNA synthesis and calculated the percentage of proliferating cells. Results showed that BrdU positive cells (BrdU⁺) are reduced in the presence of AQP4-IgG, compared to control serum (Fig. 6c). Quantification of the total number of BrdU⁺ cells effectively demonstrated that the percentage of proliferative cells is significantly reduced with the AQP4-IgG⁺ sera from the three patients (Fig. 6d). As expected, pretreatment of MIO-M1 cells with TGN-020 showed a similar reduction of BrdU incorporation. These results demonstrate that AQP4 loss from the plasma membrane altered the capacity of Müller cells to proliferate, probably by affecting fast cell volume regulation during cell division and cell cycle progression.

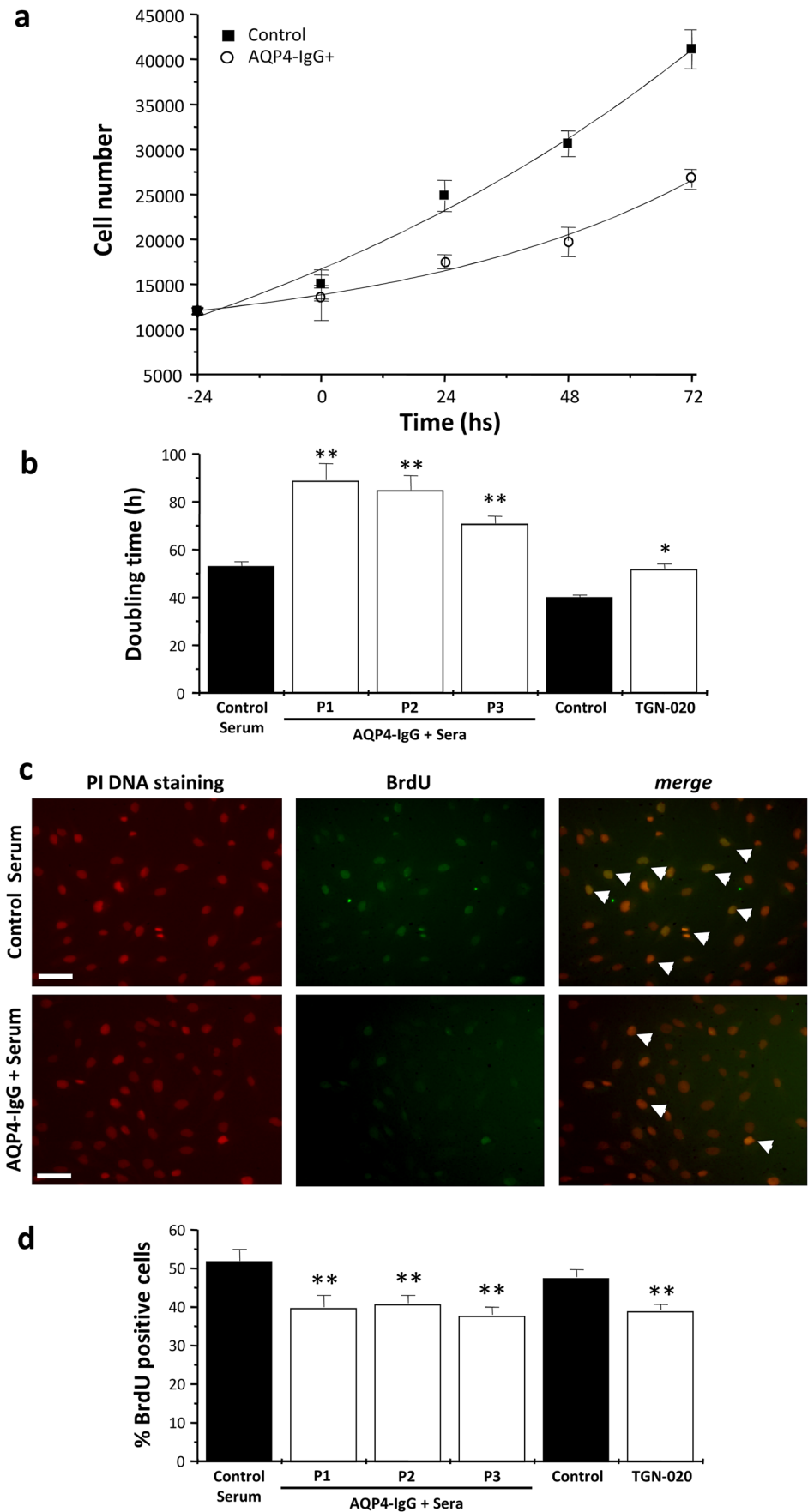
Discussion

In the present work, we confirm that AQP4 expressed in human retinal Müller cells represents a pathogenic ocular target of AQP4-IgG, as previously suggested by clinical

observations and in vitro animal models [10, 11, 40, 41]. One of the main findings of this study is that the auto-antibody binding to AQP4, before complement activation, does not directly inhibit AQP4 water permeability by blocking the water pore, but induces its partial internalization. In fact, we showed that, under conditions where membrane fluidity and metabolic processes are restricted (4 °C for 1 h), AQP4 remains in the plasma membrane and its water channel activity is not affected. This was further confirmed by comparing these results with those obtained by the use of TGN-020 inhibitor, which specifically blocks the AQP4 pore as shown by molecular dynamics studies [42]. The long-term exposure to AQP4-IgG + sera for 12 h at 37 °C, a condition that does not prevent metabolic processes, reduced AQP4 expression and induced its partial removal of the plasma membrane following the early endosomal pathway. AQP4 downregulation induced by AQP4-IgG + sera in Müller cells is in line with the report of Felix et al. (2016) [17] using a monoclonal antibody, as well as with our and others previous reports in astrocytes [34, 39]. In fact, these studies showed that while AQP4-IgG + sera induced the endocytosis of M1 isoform in astrocytes, M23 still remain in the plasma membrane, rearranging to larger OAPs. However, several other AQP4 isoforms were later described, produced by alternative splicing (AQP4b, d, e, and f) or by translational readthrough that contains a C-terminal extension (AQP4ex) [43–45]. It was proposed that AQP4ex could have an important regulatory role in OAP assembly and stability, being critical for the binding of pathogenic human AQP4-IgG autoantibodies in astrocytes [46]. In the present study, Western blot analysis for AQP4 revealed that human Müller cells express several isoforms, but the major band observed at the plasma membrane, which was partially removed after AQP4-IgG binding, is that of ~40 kDa, which may correspond to AQP4-ex. However, we cannot discard that the AQP4e isoform, a protein of also ~40 kDa present in the plasma membrane and participating in the cell volume regulation of astrocytes [47] could be also involved. The present study does not attempt to clarify this point; however, our observations support the idea that, in human Müller cells, AQP4-IgG would not bind to the canonical M1 and M23 isoforms. Future studies are needed to address this novel issue since, as previously reported, the expression of particular AQP4 isoforms depends mainly on post-transcriptional regulation, according to the specific homeostatic needs of each tissue [46].

The here observed endocytosis of AQP4 by AQP4-IgG is functionally relevant, since it leads to the decrease of plasma membrane water permeability and the impairment of one of the major roles of Müller cells, the control of the RVD response, a key mechanism to prevent detrimental swelling in response to hypo-osmotic stress in the retina. In fact, after the partial removal of AQP4 by AQP4-IgG, the changes of intracellular calcium levels, which determine the efficiency

Fig. 6 Cell proliferation of MIO-M1 cells after exposure to control or AQP4-IgG positive sera. **a–b** MIO-M1 cells were treated for 72 h at 37 °C with control or AQP4-IgG + sera and growth kinetics of cells determined by hemocytometry (**a**) and cell doubling time (**b**) obtained after fitting the individual experimental curves to exponential function. AQP4 inhibition by TGN-020 was also tested. Values are expressed as mean ± SEM, *n* = 4 experiments for each condition; ***p* < 0.01 control serum vs. AQP4-IgG + sera; **p* < 0.05 control vs. TGN-020. **c** Representative images of proliferating MIO-M1 cells. The red channel shows propidium iodide (PI) DNA staining and the green channel shows the thymidine analog 5-Bromodeoxyuridin (BrdU) staining. Proliferating cells are indicated by white arrows. Images are representative of three independent experiments (scale bars: 500 μm). **d** Percentage of BrdU positive cells in the presence of control or AQP4-IgG + sera 1, 2, and 3 evaluated by immunocytochemistry. Values are expressed as mean ± SEM, *n* = 3 experiments for each condition; ***p* < 0.01 control vs. AQP4-IgG + sera or control vs. TGN-020



of RVD mechanisms [20], were also significantly reduced. These results were further confirmed with the specific blocker of the pore of AQP4 by TGN-020. We propose an association between the presence of AQP4 with the following: (i) the activation of the RVD machinery, as the deletion of AQP4 renders mice retinal glial cells more susceptible to osmotic stress [18] and (ii) the osmotically-induced calcium signals, as previously shown in astrocytes [48], both altered in the presence of AQP4-IgG, affecting cell volume regulation response. However, AQP4-IgG does not affect neither TRPV4 expression/activity nor Vm changes occurring during cell swelling and RVD in Müller cells, indicating that the antibody affected cell volume regulation by a pathway not directly involving TRPV4. Then, how does AQP4-IgG lead to a reduction in the RVD? First, we propose that the activation of RVD effectors would be sensitive to the dynamics of cell swelling and/or its consequences (changes in membrane tension, dilution of intracellular mediators, etc.), as previously reported for some AQPs [30, 49]. Therefore, the rapid influx of water in the presence of AQP4 will lead to a faster regulation of cell volume changes by activating AQP4-dependent cell volume regulation machinery, as previously shown in mouse-cultured glial cells [50]. We cannot disregard that AQP4 endocytosis by AQP4-IgG could also induce the endocytosis of another RVD effector proteins, such as the potassium channel Kir 4.1, as previously shown to be associated with AQP4 and the distrophin complex [51].

Previous reports in mouse Müller cells described that AQP4 deletion is associated with reactive gliosis, as well as with an inflammatory response of the retinal tissue [18, 52]. We here provide experimental evidence demonstrating, for the first time, that independently of complement activation, the loss of AQP4 from the plasma membrane induced by AQP4-IgG + sera delayed the ability of Müller cells to proliferate. We also show that AQP4 inhibition with TGN-020 effectively reduced the proliferation of Müller cells without inducing cell death, directly demonstrating the contribution of AQP4 to this process. These results are in agreement with our and others studies in different cell types demonstrating that AQPs play a key role in cell volume control, an important prerequisite for the regulation of various cell properties, including proliferation, migration, and differentiation [30, 31, 53]. Even more, it was previously reported that AQP4 has a crucial role in regulating proliferation and differentiation of adult neural stem cells by its action on intracellular calcium dynamics [28]. We here show that the blockage or endocytosis of AQP4, with TGN-020 and AQP4-IgG respectively, not only altered intracellular

calcium levels during the osmotic swelling and RVD but also delayed cell proliferation. Therefore, we propose that AQP4-mediated rapid changes in cell volume and in calcium signals facilitate cell cycle progress and cell proliferation maintaining retinal homeostasis in physiological conditions (Fig. 7a). The reduction in AQP4 plasma membrane expression after binding of AQP4-IgG, decreases water permeability, affects cell volume control, and delays cell cycle, probably contributing to the physiopathology of NMOSD (Fig. 7b). In fact, this may occur in the very acute stage of NMOSD and may explain the multiple lesion patterns observed to coexist in samples from individual autopsies [54]. Shedding light on how AQP4 is able to regulate Müller cells' proliferation can increase our understanding of its biological behavior, with potential applications in regenerative and reparative medicine for NMOSD patients. In fact, stem cell transplantation has been considered to be a potential treatment method for several neurological disorders, including NMOSD, and AQPs seem to regulate the proliferation of mesenchymal stem cells (MSC) through rapid regulation of the cell volume [27, 55]. In addition, recent reports revealed that bone marrow MSC derived from patients with NMOSD exhibited a decreased proliferation rate, together with a decreased expression of several cell cycle promoting and proliferation-associated genes, compared to control healthy donors [56]. Although the mechanisms were not investigated, it is likely that changes in AQP4 expression due to the presence of AQP4-IgG could explain the differences observed in cell proliferation. The key role of AQP4 on cell proliferation might also explain the *in vivo* reported structural and functional Müller cells' dysfunction observed, by full-field electroretinography and spectral-domain OCT, only in NMOSD patients who were AQP4-IgG positive [57]. Further studies are warranted to investigate these mechanisms and its potential implications for the prognosis and treatment of optic neuritis in NMOSD.

In conclusion, we here propose that AQP4-IgG present in the sera of NMOSD patients causes the removal of endogenously expressed AQP4 from the plasma membrane of retinal Müller cells, affecting osmotic water permeability, the consequent activation of the cell volume regulation machinery and cell proliferation. Since all experiments were performed in the absence of active complement, we can hypothesize that AQP4 removal from the plasma membrane by AQP4-IgG binding could be a non-inflammatory mechanism of retinal injury *in vivo*, altering cell volume homeostasis and retinal regeneration of Müller cells, contributing to the physiopathology of NMOSD.

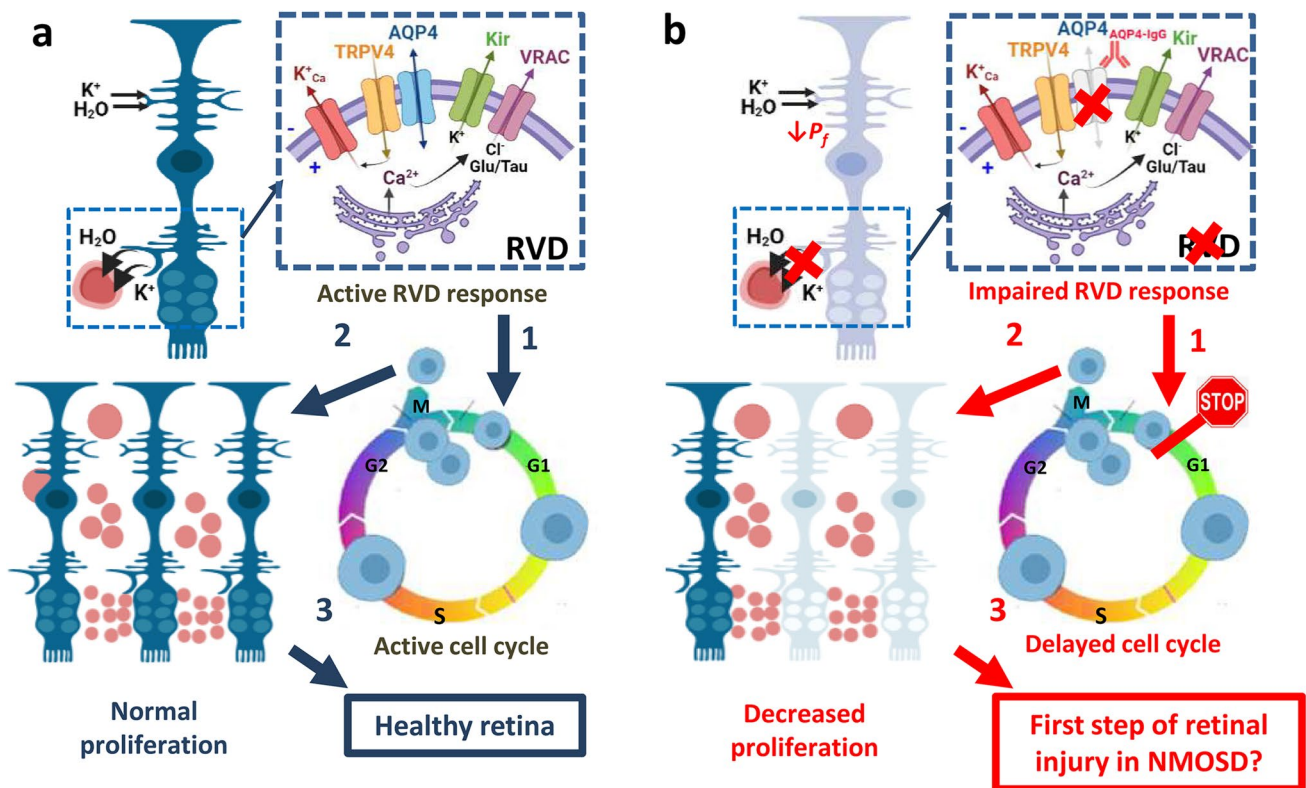


Fig. 7 Proposed model to explain the complement-independent dysfunction of Müller cells after AQP4-IgG binding to AQP4. **a** In physiological conditions, neural activity induces water and K^+ uptake and cell swelling, which is followed by RVD response. RVD is a complex mechanism that involves AQP4 and TRPV4-dependent changes in membrane potential (V_m) as well as the activation of K^+ and Cl^- channels and the release of Taurine (Tau) and Glutamate (Glu) via VRAC (left upper panel). RVD capacity is also actively modu-

lated during G0/G1 phase of cell cycle and plays an important role in cell cycle progress (1) to promote cell proliferation (2) and maintain retinal homeostasis (3). **b** In the presence of AQP4-IgG in NMOSD, AQP4 is partially removed from the plasma membrane and the activation of the AQP4-dependent RVD response is affected, resulting in Müller cells' dysfunction (right upper panel). Consequently, cell cycle is delayed (1) and the rate of cell proliferation decreases (2), probably contributing to the pathophysiology of NMOSD in the retina (3)

Acknowledgements The authors thank Dr. Astrid Limb (University College London, London, UK) for providing the human Müller Cell Line (MIO-M1) and Natalia Beltramone, Germán La Iacona, and Ricardo Dorr for technical assistance.

Author Contribution Claudia Capurro and Vanina Netti designed the study, interpreted the data, and coordinated the project. Vanina Netti and Juan Fernández conducted the experiments, data collection, and statistical analysis. Luciana Melamud provided consultation for clinical relevance. Pablo García-Miranda and Gisela Di Justo provided consultation for methodology and conducted some experiments. Paula Ford and Miriam Echevarria contributed to the design stages and interpretation of the research. The manuscript was written by Claudia Capurro and Vanina Netti and all authors commented on previous versions of the manuscript. All authors read and approved the final manuscript.

Funding This study was supported by grants from the University of Buenos Aires (UBA-SECYT, 20020130100682BA, 2018–2021, Argentina) to Claudia Capurro; the Agencia Nacional de Promoción Científica y Tecnológica (ANPCyT 2019–01707, Argentina) to Claudia Capurro and the Spanish Ministry of Economy and Competitiveness, co-financed by the Carlos III Health Institute (ISCIII)

and European Regional Development Fund (FEDER, PI16/00493) to Miriam Echevarria.

Data Availability The datasets generated and/or analyzed during the current study are available upon reasonable request.

Declarations

Ethics Approval The study was approved by the Institutional Ethics Committee for Research in Translational Medicine Alberto C. Taquini of the School of Medicine, University of Buenos Aires (IATIMET, N°: PICT2019/10707 version 1.0), which is in compliance with the International Guideline for Human Research protection as laid down in the 1964 Declaration of Helsinki and its later amendments or comparable ethical standards.

Consent to Participate Informed consent was obtained from all individual participants included in the study.

Consent for Publication Not applicable.

Conflict of Interest The authors declare no conflict of interest.

References

- Pittock SJ, Lucchinetti CF (2016) Neuromyelitis optica and the evolving spectrum of autoimmune aquaporin-4 channelopathies: a decade later. *Ann N Y Acad Sci* 1366(1):20–39. <https://doi.org/10.1111/nyas.12794>
- Lennon VA, Wingerchuk DM, Kryzer TJ, Pittock SJ, Lucchinetti CF, Fujihara K, Nakashima I, Weinshenker BG (2004) A serum autoantibody marker of neuromyelitis optica: distinction from multiple sclerosis. *Lancet* 364:2106–2112. [https://doi.org/10.1016/S0140-6736\(04\)17551-X](https://doi.org/10.1016/S0140-6736(04)17551-X)
- Lennon VA, Kryzer TJ, Pittock SJ, Verkman AS, Hinson SR (2005) IgG marker of optic-spinal multiple sclerosis binds to the aquaporin-4 water channel. *J Exp Med* 202:473–477. <https://doi.org/10.1084/jem.20050304>
- Nagelhus EA, Ottersen OP (2013) Physiological roles of aquaporin-4 in brain. *Physiol Rev* 93:1543–1562. <https://doi.org/10.1152/physrev.00011.2013>
- Bradl M, Reindl M, Lassmann H (2018) Mechanisms for lesion localization in neuromyelitis optica spectrum disorders. *Curr Opin Neurol* 31:325–333. <https://doi.org/10.1097/WCO.0000000000000551>
- Chang VTW, Chang HM (2020) Recent advances in the understanding of the pathophysiology of neuromyelitis optica spectrum disorder. *Neuropathol Appl Neurobiol* 46:199–218. <https://doi.org/10.1111/nan.12574>
- Ratelade J, Verkman AS (2012) Neuromyelitis optica: aquaporin-4 based pathogenesis mechanisms and new therapies. *Int J Biochem Cell Biol* 44:1519–1530. <https://doi.org/10.1016/j.biocel.2012.06.013>
- Bennett JL, Owens GP (2017) Neuromyelitis optica: deciphering a complex immune-mediated astrocytopathy. *J Neuroophthalmol* 37:291–299. <https://doi.org/10.1097/WNO.0000000000000508>
- Reichenbach A, Bringmann A (2020) Glia of the human retina. *Glia* 68:768–796. <https://doi.org/10.1002/glia.23727>
- Gelfand JM, Cree BA, Nolan R, Arnow S, Green AJ (2013) Microcystic inner nuclear layer abnormalities and neuromyelitis optica. *JAMA Neurol* 70:629–633. <https://doi.org/10.1001/jamaneurol.2013.1832>
- Sotirchos ES, Saidha S, Byraiah G, Mealy MA, Ibrahim MA, Sepah YJ, Newsome SD, Ratchford JN et al (2013) In vivo identification of morphologic retinal abnormalities in neuromyelitis optica. *Neurology* 80:1406–1414. <https://doi.org/10.1212/WNL.0b013e31828c2f7a>
- Bennett JL, de Seze J, Lana-Peixoto M, Palace J, Waldman A, Schippling S, Tenenbaum S, Banwell B et al (2015) Neuromyelitis optica and multiple sclerosis: Seeing differences through optical coherence tomography. *Mult Scler* 21:678–688. <https://doi.org/10.1177/1352458514567216>
- Peng C, Wang W, Xu Q, Zhao S, Li H, Yang M, Cao S, Zhou H et al (2016) Structural alterations of segmented macular inner layers in aquaporin4-antibody-positive optic neuritis patients in a Chinese population. *PLoS One* 11(6):e0157645. <https://doi.org/10.1371/journal.pone.0157645>
- Oertel FC, Kuchling J, Zimmermann H, Chien C, Schmidt F, Knier B, Bellmann-Strobl J, Korn T et al (2017) Microstructural visual system changes in AQP4-antibody-seropositive NMOSD. *Neurol Neuroimmunol Neuroinflamm* 4(3):e334. <https://doi.org/10.1212/NXI.0000000000000334>
- Filippatou AG, Vasileiou ES, He Y, Fitzgerald KC, Kalaitzidis G, Lambe J, Mealy MA, Levy M et al (2020) Evidence of subclinical quantitative retinal layer abnormalities in AQP4-IgG seropositive NMOSD. *Mult Scler*. <https://doi.org/10.1177/1352458520977771>
- Zeka B, Hastermann M, Kaufmann N, Schanda K, Pende M, Misu T, Rommer P, Fujihara K et al (2016) Aquaporin 4-specific T cells and NMO-IgG cause primary retinal damage in experimental NMO/SD. *Acta Neuropathol Commun* 4(1):82. <https://doi.org/10.1186/s40478-016-0355-y>
- Felix CM, Levin MH, Verkman AS (2016) Complement-independent retinal pathology produced by intravitreal injection of neuromyelitis optica immunoglobulin G. *J Neuroinflammation* 13(1):275. <https://doi.org/10.1186/s12974-016-0746-9>
- Pannicke T, Wurm A, Iandiev I, Hollborn M, Linnertz R, Binder DK, Kohen L, Wiedemann P et al (2010) Deletion of aquaporin-4 renders retinal glial cells more susceptible to osmotic stress. *J Neurosci Res* 88:2877–2888. <https://doi.org/10.1002/jnr.22437>
- Fernández JM, Di Giusto G, Kalstein M, Melamud L, Rivarola V, Ford P, Capurro C (2013) Cell volume regulation in cultured human retinal Müller cells is associated with changes in transmembrane potential. *PLoS One* 8(2):e57268. <https://doi.org/10.1371/journal.pone.0057268>
- Netti V, Fernández J, Kalstein M, Pizzoni A, Di Giusto G, Rivarola V, Ford P, Capurro C (2017) TRPV4 contributes to resting membrane potential in retinal müller cells: implications in cell volume regulation. *J Cell Biochem* 118(8):2302–2313. <https://doi.org/10.1002/jcb.25884>
- Netti V, Pizzoni A, Pérez-Domínguez M, Ford P, Pasantes-Morales H, Ramos-Mandujano G, Capurro C (2018) Release of taurine and glutamate contributes to cell volume regulation in human retinal Müller cells: differences in modulation by calcium. *J Neurophysiol* 120(3):973–984. <https://doi.org/10.1152/jn.00725.2017>
- Benfenati V, Caprini M, Dovizio M, Mylonakou MN, Ferroni S, Ottersen OP, Amiry-Moghaddam M (2011) An aquaporin-4/transient receptor potential vanilloid 4 (AQP4/TRPV4) complex is essential for cell-volume control in astrocytes. *Proc Natl Acad Sci* 108(6):2563–2568. <https://doi.org/10.1073/pnas.1012867108>
- Jo AO, Ryskamp DA, Phuong TT, Verkman AS, Yarishkin O, MacAulay N, Križaj D (2015) TRPV4 and AQP4 channels synergistically regulate cell volume and calcium homeostasis in retinal müller glia. *J Neurosci* 35(39):13525–13537. <https://doi.org/10.1523/JNEUROSCI.1987-15.2015>
- Fischer A, Reh T (2001) Müller glia are a potential source of neural regeneration in the postnatal chicken retina. *Nat Neurosci* 4:247–252. <https://doi.org/10.1038/85090>
- Ooto S, Akagi T, Kageyama R, Akita J, Mandai M, Honda Y, Takahashi M (2004) Potential for neural regeneration after neurotoxic injury in the adult mammalian retina. *Proc Natl Acad Sci* 101(37):13654–13659. <https://doi.org/10.1073/pnas.0402129101>
- Giaume C, Kirchhoff F, Matute C, Reichenbach A, Verkhratsky A (2007) Glia: the fulcrum of brain diseases. *Cell Death Differ* 14(7):1324–1335. <https://doi.org/10.1038/sj.cdd.4402144>
- Greco R, Bondanza A, Vago L, Muiola L, Rossi P, Furlan R, Martino G, Radaelli M et al (2014) Allogeneic hematopoietic stem cell transplantation for neuromyelitis optica. *Ann Neurol* 75(3):447–453. <https://doi.org/10.1002/ana.24079>
- Kong H, Fan Y, Xie J, Ding J, Sha L, Shi X, Sun X, Hu G (2008) AQP4 knockout impairs proliferation, migration and neuronal differentiation of adult neural stem cells. *J Cell Sci* 121(Pt 24):4029–4036. <https://doi.org/10.1242/jcs.035758>
- Li YB, Sun SR, Han XH (2016) Down-regulation of AQP4 inhibits proliferation, migration and invasion of human breast cancer cells. *Folia Biol (Praga)* 62(3):131–137
- Di Giusto G, Flamenco P, Rivarola V, Fernández J, Melamud L, Ford P, Capurro C (2012) Aquaporin 2-increased renal cell proliferation is associated with cell volume regulation. *J Cell Biochem* 113(12):3721–3729. <https://doi.org/10.1002/jcb.24246>

31. Galán-Cobo A, Ramírez-Lorca R, Echevarría M (2016) Role of aquaporins in cell proliferation: What else beyond water permeability? *Channels* 10(3):185–201. <https://doi.org/10.1080/19336950.2016.1139250>
32. Limb GA, Salt TE, Munro PM, Moss SE, Khaw PT (2002) In vitro characterization of a spontaneously immortalized human Muller cell line (MIO-M1). *Invest Ophthalmol Vis Sci* 43:864–869
33. Wingerchuk DM, Banwell B, Bennett JL, Cabre P, Carroll W, Chitnis T, de Seze J, Fujihara K et al (2015) International consensus diagnostic criteria for neuromyelitis optica spectrum disorders. *Neurology* 85(2):177–189. <https://doi.org/10.1212/WNL.0000000000001729>
34. Melamud L, Fernandez JM, Rivarola V, Di Giusto G, Ford P, Villa A, Capurro C (2012) Neuromyelitis Optica Immunoglobulin G present in sera from neuromyelitis optica patients affects aquaporin-4 expression and water permeability of the astrocyte plasma membrane. *J Neurosci Res* 90:1240–1248. <https://doi.org/10.1002/jnr.22822>
35. García-Miranda P, Morón-Civanto FJ, Martínez-Olivo MDM, Suárez-Luna N, Ramírez-Lorca R, Lebrato-Hernández L, Lamas-Pérez R, Navarro G et al (2019) Predictive value of serum antibodies and point mutations of AQP4, AQP1 and MOG in a cohort of Spanish patients with neuromyelitis optica spectrum disorders. *Int J Mol Sci* 20(22):5810. <https://doi.org/10.3390/ijms20225810>
36. Hinson SR, Pittock SJ, Lucchinetti CF, Roemer SF, Fryer JP, Kryzer TJ, Lennon VA (2007) Pathogenic potential of IgG binding to water channel extracellular domain in neuromyelitis optica. *Neurology* 69:2221–2231. <https://doi.org/10.1212/01.WNL.0000289761.64862.ce>
37. Kida T, Oku H, Horie T, Fukumoto M, Okuda Y, Morishita S, Ikeda T (2017) Implication of VEGF and aquaporin 4 mediating Müller cell swelling to diabetic retinal edema. *Graefes Arch Clin Exp Ophthalmol* 255(6):1149–1157. <https://doi.org/10.1007/s00417-017-3631-z>
38. Sachs AN, Pisitkun T, Hoffert JD, Yu MJ, Knepper MA (2008) LC-MS/MS analysis of differential centrifugation fractions from native inner medullary collecting duct of rat. *Am J Physiol Renal Physiol* 295(6):F1799–F1806. <https://doi.org/10.1152/ajprenal.90510.2008>
39. Hinson SR, Romero MF, Popescu BF, Lucchinetti CF, Fryer JP, Wolburg H, Fallier-Becker P, Noell S et al (2012) Molecular outcomes of neuromyelitis optica (NMO)-IgG binding to aquaporin-4 in astrocytes. *Proc Natl Acad Sci* 109(4):1245–1250. <https://doi.org/10.1073/pnas.1109980108>
40. Green AJ, Cree BA (2009) Distinctive retinal nerve fibre layer and vascular changes in neuromyelitis optica following optic neuritis. *J Neurol Neurosurg Psychiatry* 80(9):1002–1005. <https://doi.org/10.1136/jnnp.2008.166207>
41. Levin MH, Bennett JL, Verkman AS (2013) Optic neuritis in neuromyelitis optica. *Prog Retin Eye Res* 36:159–171. <https://doi.org/10.1016/j.preteyeres.2013.03.001>
42. Toft-Bertelsen TL, Larsen BR, Christensen SK, Khandelia H, Waagepetersen HS, MacAulay N (2020) Clearance of activity-evoked K⁺ transients and associated glia cell swelling occur independently of AQP4: a study with an isoform-selective AQP4 inhibitor. *Glia* 69(1):28–41. <https://doi.org/10.1002/glia.23851>
43. De Bellis M, Pisani F, Mola MG, Rosito S, Simone L, Buccoliero C, Trojano M, Nicchia GP et al (2017) Translational readthrough generates new astrocyte AQP4 isoforms that modulate supramolecular clustering, glial endfeet localization, and water transport. *Glia* 65(5):790–803. <https://doi.org/10.1002/glia.23126>
44. Lisjak M, Potokar M, Zorec R, Jorgačevski J (2020) Indirect Role of AQP4b and AQP4d Isoforms in Dynamics of Astrocyte Volume and Orthogonal Arrays of Particles. *Cells* 9(3):735. <https://doi.org/10.3390/cells9030735>
45. Jorgačevski J, Zorec R, Potokar M (2020) Insights into Cell Surface Expression, Supramolecular Organization, and Functions of Aquaporin 4 Isoforms in Astrocytes. *Cells* 9(12):2622. <https://doi.org/10.3390/cells9122622>
46. Palazzo C, Buccoliero C, Mola MG, Abbrescia P, Nicchia GP, Trojano M, Frigeri A (2019) AQP4ex is crucial for the anchoring of AQP4 at the astrocyte end-feet and for neuromyelitis optica antibody binding. *Acta Neuropathol Commun* 7(1):51. <https://doi.org/10.1186/s40478-019-0707-5>
47. Lisjak M, Potokar M, Rituper B, Jorgačevski J, Zorec R (2017) AQP4e-based orthogonal arrays regulate rapid cell volume changes in astrocytes. *J Neurosci* 37(44):10748–10756. <https://doi.org/10.1523/JNEUROSCI.0776-17.2017>
48. Thrane AS, Rappold PM, Fujita T, Torres A, Bekar LK, Takano T, Peng W, Wang F et al (2010) Critical role of aquaporin-4 (AQP4) in astrocytic Ca²⁺ signaling events elicited by cerebral edema. *Proc Natl Acad Sci* 108(2):846–851. <https://doi.org/10.1073/pnas.1015217108>
49. Galizia L, Flamenco MP, Rivarola V, Capurro C, Ford P (2008) Role of AQP2 in activation of calcium entry by hypotonicity: implications in cell volume regulation. *Am J Physiol Renal Physiol* 294(3):F582–F590. <https://doi.org/10.1152/ajprenal.00427.2007>
50. Mola MG, Sparaneo A, Gargano CD, Spray DC, Svelto M, Frigeri A, Scemes E, Nicchia GP (2016) The speed of swelling kinetics modulates cell volume regulation and calcium signaling in astrocytes: a different point of view on the role of aquaporins. *Glia* 64(1):139–154. <https://doi.org/10.1002/glia.22921>
51. Fort PE, Sene A, Pannicke T, Roux MJ, Forster V, Mornet D, Nudel U, Yaffe D et al (2008) Kir4.1 and AQP4 associate with Dp71- and utrophin-DAPs complexes in specific and defined microdomains of Müller retinal glial cell membrane. *Glia* 56(6):597–610. <https://doi.org/10.1002/glia.20633>
52. Nicchia GP, Pisani F, Simone L, Cibelli A, Mola MG, Dal Monte M, Frigeri A, Bagnoli P et al (2016) Glio-vascular modifications caused by Aquaporin-4 deletion in the mouse retina. *Exp Eye Res* 146:259–268. <https://doi.org/10.1016/j.exer.2016.03.019>
53. Di Giusto G, Pizzoni A, Rivarola V, Beltramone N, White A, Ford P, Capurro C (2019) Aquaporin-2 and Na⁺/H⁺ exchanger isoform 1 modulate the efficiency of renal cell migration. *J Cell Physiol* 235(5):4443–4454. <https://doi.org/10.1002/jcp.29320>
54. Takai Y, Misu T, Suzuki H, Takahashi T, Okada H, Tanaka S, Okita K, Sasou S et al (2021) Staging of astrocytopathy and complement activation in neuromyelitis optica spectrum disorders. *Brain*. <https://doi.org/10.1093/brain/awab102>
55. Zannetti A, Benga G, Brunetti A, Napolitano F, Avallone L, Pelagalli A (2020) Role of Aquaporins in the Physiological Functions of Mesenchymal Stem Cells. *Cells* 9(12):2678. <https://doi.org/10.3390/cells9122678>
56. Yang C, Yang Y, Ma L, Zhang GX, Shi FD, Yan Y, Chang G (2019) Study of the cytological features of bone marrow mesenchymal stem cells from patients with neuromyelitis optica. *Int J Mol Med* 43(3):1395–1405. <https://doi.org/10.3892/ijmm.2019.4056>
57. You Y, Zhu L, Zhang T, Shen T, Fontes A, Yiannikas C, Parratt J, Barton J et al (2019) Evidence of Müller glial dysfunction in patients with aquaporin-4 immunoglobulin g-positive neuromyelitis optica spectrum disorder. *Ophthalmology* 126(6):801–810. <https://doi.org/10.1016/j.ophtha.2019.01.016>

Publisher's Note Springer Nature remains neutral with regard to jurisdictional claims in published maps and institutional affiliations.